On the Development of Spiral Bands in a Tropical Cyclone

YOSHIO KURIHARA

Geophysical Fluid Dynamics Laboratory/NOAA, Princeton University, Princeton, N. J. 08540

(Manuscript received 4 August 1975, in revised form 22 January 1976)

ABSTRACT

Development of the band structure in a tropical cyclone is investigated by solving an eigenvalue problem for perturbations of spiral shape. The perturbations are superposed on a baroclinic circular vortex accompanied with a radial and vertical basic flow.

It is shown that the spiral bands in three different modes may be intensified in an inner area of a tropical cyclone. The baroclinicity of a basic field is not required for the development of bands in any mode. A spiral band which propagates outward can grow in the presence of the horizontal shear of the basic azimuthal flow. Without the basic circular vortex, this band is reduced to a neutral gravity-inertia wave with a particular vertical structure. The unstable spiral in this mode takes a pattern which extends clockwise from the center of a storm in the Northern Hemisphere. An azimuthal wavenumber 2 and a radial scale (twice the band width) of 200 km are preferred by this band. Another band with the characteristics of an inward propagating gravity wave may be excited in an inner area of a storm by its strong response to the effect of diabatic heating. The third kind of band has the features of a geostrophic mode and moves inward. Its development in an inner area is associated with the horizontal shear of the basic circular flow. The bands of the second and the third mode have not been observed in real storms. Dynamical behavior as well as the energetics of a band are discussed for each mode.

There exists practically no instability in the outer region of the storm for any kind of spiral band. It is speculated that a band which grows in an inner area and propagates outward, i.e., the band of the first mode mentioned above, may become a neutral spiral while moving toward the outer region. Some of the outer spiral bands observed in real tropical cyclones may be interpreted as this kind of internal gravity-inertia waves.

1. Introduction

The results of an investigation on the development, structure and behavior of spiral bands in a tropical cyclone are presented in this paper. Eigenvalue solutions are obtained for perturbations of spiral shape which are superposed on the basic axisymmetric field representing a tropical cyclone.

The banded structure of hurricanes and typhoons has been noted in several observational studies where radar or aircraft data have been available and, in some cases, by correlating these data with mesosynoptic data (e.g., Wexler, 1947; Simpson, 1954; Ligda, 1955; Senn and Hiser, 1959; Tatehira, 1961; Atlas *et al.*, 1963). The analysis by the Staff Members of Tokyo University (1969, 1970) revealed the banded distribution in the time variation of rainfall intensity. Satellite observations have also been used in considering a model including bands (e.g., Fett, 1964; Fujita *et al.*, 1967). It is suggested in some, but not all, of these analyses that the spiral bands in a tropical cyclone behave like gravity waves. Tepper (1958) and Abdullah (1966) hypothesized that the bands are gravity waves similar to pressure jumps. Similarity to shallow water waves has also been suggested to explain the bands (Arakawa and Manabe, 1963). In his study of the Ekman layer instability, Faller (1961) proposed an experimental analogy with the hurricane spiral bands. The question concerning a possible role of the Ekman layer instability in the formation of bands will remain unanswered in the present study, because the boundary layer will not be adequately resolved by the hurricane model of this paper.

In recent years, it has been shown that the banded structure of a tropical cyclone may develop in three-dimensional numerical models. Anthes (1972) made an analysis of the asymmetries in his model and suggested a possible relationship between the bands, which he mentioned were internal gravity waves, and the eddies in the upper outflow layer. Kurihara and Tuleya (1974) examined the phase relationships among the various meteorological quantities in the outer area of their simulated tropical cyclone. They found the features of internal gravity waves in the band structure. In their study on the energetics of the above model, Tuleya and Kurihara (1975) mentioned the possibility of the coexistence of two distinct kinds of eddies in the inner region which receive energy, respectively, from the kinetic energy of the basic flow and from the total potential energy.

In the simulation experiments cited above, the initial field for the numerical integration was axi-

symmetric. The simplified models did not include the effect of the latitudinal variation of the Coriolis parameter. Mathur (1975) included this effect in his model and made the integration starting from the observed asymmetric initial field. The stationary and the clockwise propagating bands developed in his model. The shape and the structure of these bands were different from those formed in the models by Anthes (1972) and Kurihara and Tuleya (1974). He concluded that development of the propagating bands in his model is related to the release of latent heat in the upper troposphere. This seems to suggest that many different factors may contribute to the formation of various kinds of bands, some of which may not necessarily take spiral shape.

This paper will deal with a problem concerning the intensification of spiral bands of a tropical cyclone in the presence of the basic axisymmetric flow. The problem is posed in the form of an eigenvalue problem. In Section 2, the perturbation equations are introduced and the basic states are specified. In Section 3, the perturbation fields of spiral shape are classified into three basic modes according to the physical characteristics of the eigensolutions for the simplified conditions. Then, separately for each mode, the role of different physical factors in the growth of bands is examined by changing the level of sophistication of the system of equations, and the preferred spiral pattern and scale are discussed. In Section 7, the energetics of the spiral bands are presented. Although the present approach to the problem is somewhat crude, the analysis results would be hopefully heuristic and informative in interpreting the spiral bands.

2. Perturbation equations and basic state

a. Perturbation equations

The linearized equations for small perturbations superposed on a basic axisymmetric meteorological field are given for a cylindrical-pressure coordinate system. These equations are as follows:

EQUATION OF MOTION

$$\frac{\partial u}{\partial t}=-U\frac{\partial u}{\partial r}-u\frac{\partial U}{\partial r}-V\frac{\partial u}{R\partial\varphi}-W\frac{\partial u}{\partial p}-\omega\frac{\partial U}{\partial p}+\left(f+\frac{2V}{R}\right)v-\frac{\partial\phi}{\partial r}+{}_HF_u+{}_VF_u \quad (2.1)$$

$$\frac{\partial v}{\partial t}=-U\frac{\partial v}{\partial r}-u\frac{\partial V}{\partial r}-V\frac{\partial v}{R\partial\varphi}-W\frac{\partial v}{\partial p}-\omega\frac{\partial V}{\partial p}-\left(f+\frac{V}{R}\right)u-\frac{U}{R}v-\frac{\partial\phi}{R\partial\varphi}+{}_HF_v+{}_VF_v. \quad (2.2)$$

Here t is time, r the radius, φ the azimuthal angle, p the pressure, and f the Coriolis parameter. The basic flow consists of the radial (outward) and the azimuthal (counterclockwise) component of horizontal wind and the vertical p-velocity, i.e., U, V and W, respectively. The corresponding perturbation flow is denoted by u, v and ω, respectively. The perturbation geopotential for an isobaric surface is expressed by ϕ. The last two terms in (2.1) and (2.2) represent the effects of horizontal and vertical diffusion of u and v, respectively. As indicated by the third term on the right-hand side of the equations, the angular velocity at the reference radius R is used for the azimuthal advection. The effect of differential azimuthal advection will be included, in the next section, in the terms for the horizontal diffusion.

All the coefficients of the above equations are given as functions of pressure only. Note that $\partial U/\partial r$ and $\partial V/\partial r$ also appear as coefficients for certain terms, although the coefficients U and V are treated as being invariable with respect to radius. This is done in order to include the effect of the horizontal shear of the basic flow which is of possible importance.

The basic flow field in an actual tropical cyclone varies with radius. A band may behave differently at various radii. In this study, this situation is dealt with as follows. At first, a certain value is chosen for a reference radius and a set of coefficients of the perturbation equations is derived from the observed meteorological fields at this radius of a tropical cyclone. The equations are solved for this case. Next, specifying another reference radius, the other set of coefficients is determined similarly and the solution for the equations with these coefficients is obtained. Now, each of the two obtained solutions is assumed to be valid only in the vicinity of the corresponding reference radius. If the difference in the two solutions is small, a perturbation is supposed to undergo a gradual change from one radius to the other.

The validity of the above strategy depends on the basic features of real tropical cyclones as well as the radial scale of disturbances to be analyzed. As mentioned before, the coefficients of the perturbation equations are treated as functions of pressure alone. This assumption may be tolerable when a certain condition of the basic field, which contributes predominantly to the determination of the dynamical behavior of the perturbation, varies slowly for a radial range comparable to the radial scale of the bands. It will turn out later that the radial shear of basic flow is an important factor. Then, if the radial shear does not change very much for an appropriate radial range near a reference radius, the coefficients of the perturbation equations may be approximated by the values at the reference radius. In the present study, two solutions are obtained for two reference radii, where the basic states are different from each other, but not drastically. Comparison of two solutions may

be one way to check the present scheme. If the solutions at two radii are quite different, it may mean inappropriateness of the analysis method. This did not happen in this study. Thus, in spite of the limitation to its utilization, it is hoped that the present method yields meaningful results.

TENDENCY EQUATION

The change in geopotential height of the lowest pressure surface, which is 1000 mb in the present model, is related to ω at that level by the relation

$$\frac{\partial \phi_s}{\partial t}=-U\frac{\partial \phi_s}{\partial r}-u\frac{\partial \Phi_s}{\partial r}-V\frac{\partial \phi_s}{R\partial \varphi}+\omega\frac{R_g T}{p}. \quad (2.3)$$

Here Φ_s represents geopotential of the basic 1000 mb surface, R_g the gas constant and T the temperature. The relation (2.3) is equivalent to the condition that the vertical motion vanishes at the surface, as will be explained in Section 3b.

CONTINUITY EQUATION

$$\frac{\partial u}{\partial r}+\frac{u}{R}+\frac{\partial v}{R\partial \varphi}+\frac{\partial \omega}{\partial p}=0. \quad (2.4)$$

HYDROSTATIC RELATION

The hydrostatic relation is assumed to hold:

$$\frac{\partial \phi}{\partial \ln p}=-R_g\theta\left(\frac{p}{p_{00}}\right)^{\kappa}. \quad (2.5)$$

Here θ is the perturbation potential temperature, $p_{00}=1000$ mb, and $\kappa=R_g/c_p$ where c_p is the specific heat of air at constant pressure.

THERMODYNAMIC EQUATION

$$\frac{\partial \theta}{\partial t}=-U\frac{\partial \theta}{\partial r}-u\frac{\partial \Theta}{\partial r}-V\frac{\partial \theta}{R\partial \varphi}-W\frac{\partial \theta}{\partial p}-\omega\frac{\partial \Theta}{\partial p}+{}_HF_\theta+q. \quad (2.6)$$

Here Θ is the potential temperature of the basic field. The last two terms are the effects of horizontal diffusion and of diabatic heating, respectively. The formulas for those terms as well as those for the effects of diffusion in (2.1) and (2.2) will be given in the next section.

b. Perturbations of spiral shape

In the present study, a functional form for expressing the perturbation field is given *a priori*. Specifically, noting the leading term in the asymptotic series used to represent the Bessel function for large arguments (e.g., Lamb, 1932), the following form is chosen for describing a perturbation field of spiral shape:

$$x=A\left(\frac{r}{R}\right)^{-\frac{1}{2}}\exp\left[i\left(m\varphi\pm\frac{2\pi}{D}r-\sigma t\right)\right], \quad (2.7)$$

where x stands for a perturbation quantity. In the above form, the radial argument is expressed by $2\pi r/D$ where D is the radial wavelength. The case with $r=150$ km and $D=200$ km will be discussed often later. The argument for this case is 4.7. The Bessel function for this argument can be approximated fairly well by the leading term of asymptotic expansion. It is anticipated that, when the argument is not small, a solution to be obtained in the above form would be a good approximation to the rigorous solution for the perturbation equations and suitable boundary conditions.

In (2.7), A is the complex amplitude at the radius R and is a function of the vertical coordinate. It is to be determined as an eigensolution in the following analysis. The physical requirement that the kinetic and the available potential energy along a radius circle must be preserved for a radially propagating neutral perturbation is satisfied by the amplitude variation factor $(r/R)^{-\frac{1}{2}}$. For small r, x may become very large because of a relaxed condition implied by (2.7). However, a small central area is excluded from the region of interest. As mentioned before, an obtained solution will be regarded as valid only in the neighborhood of the reference radius R. The scale of a spiral band is determined by the azimuthal wavenumber m and the radial wavelength D. For a given combination of m and D, there exist two spirals with different orientation depending on the sign $\pm$ in (2.7); the plus sign requires a spiral to extend clockwise from the center, which will be called an N-type spiral, and the negative sign yields an S-type spiral which extends counterclockwise. The schematic patterns of spirals, both N-type and S-type, for the different wavenumbers are shown in Fig. 1. The areas of negative value are shaded. The actual observations suggest that the spirals of N-type are typical in the Northern Hemisphere, and the S-type in the Southern Hemisphere. The angle with which a constant-phase line intersects a circle of radius r is easily obtained:

$$B=\arctan\left(\frac{mD}{2\pi r}\right). \quad (2.8)$$

A complex number σ in (2.7), which is to be obtained as an eigenvalue from the condition that the amplitudes of perturbations are non-zero, represents the frequency σ_r as well as the growth rate σ_i, i.e., $\sigma=\sigma_r+i\sigma_i$. In other words, $2\pi/\sigma_r$ gives the period

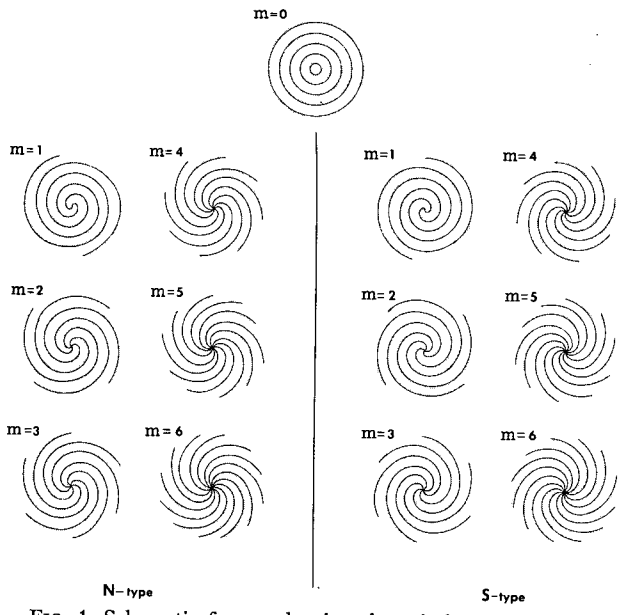

FIG. 1. Schematic figures showing the spiral patterns for different azimuthal wavenumber m. Negative areas of perturbations are shaded. Both the N-type and S-type spiral patterns are shown.

during which a phase of perturbation propagates by one complete cycle; and $1/\sigma_i$ is the so-called e-folding time. When $\sigma_r>0$, a constant-phase line propagates counterclockwise and outward for an N-type spiral, and counterclockwise and inward for an S-type spiral. However, if $\sigma_r<0$, it moves clockwise so that a spiral appears to converge for the N-type pattern and to diverge for the S-type. In the Northern Hemisphere, the actually observed outer spiral bands move as N-type spirals with $\sigma_r>0$.

In the present analysis, the perturbation equations (2.1)–(2.6) are applied to discrete pressure levels. In case of a perturbation of the form (2.7), its time and horizontal derivative are expressed as $\partial/\partial t=-i\sigma$, $\partial/\partial\varphi=im$ and $\partial/\partial r=\pm i(2\pi/D)-(2r)^{-1}$. If the vertical derivative of a perturbation quantity is replaced by vertical finite differencing, then a system of homogeneous equations for the perturbation amplitudes is derived. The solutions are, of course, nontrivial only when σ takes proper values for a given basic field and for the specified values of m and D.

In Table 1, the pressure levels where the perturbation variables are defined are listed. There are 28 variables in total. Eqs. (2.1), (2.2) and (2.6) are applied to the levels for which u, v and θ are assigned, respectively. The variation of ϕ at 1000 mb is governed by (2.3). The hydrostatic relation (2.5) is applied to a layer between 1000 and 900 mb and also to four layers, each 200 mb thick, between 900 and 100 mb. The continuity equation (2.4) is used for each of four 200 mb intervals between 1000 and 200 mb, and also for a layer between 200 and 100 mb. At 100 mb, ω is set to be half of that at 200 mb. The equation system can be closed with the above 18 prognostic equations and 10 diagnostic formulas. The number of eigenvalues is therefore 18 for a given set of parameters which determine the scale and type of a spiral. In the present study, a specially prepared computer program was used to obtain the eigenvalues and the corresponding eigensolutions.

A careful formulation of the vertical finite differencing is required in the present problem since the vertical resolution is coarse. Also, the calculated solutions with many nodes in the vertical are not stressed since their numerical reliability is considered poor. Some remarks on the numerical schemes used in the present analysis are given in Appendix A.

c. *Basic field*

Basic meteorological fields are specified for the two reference radii, $R=150$ km and $R=400$ km. The field at 150 km radius represents a strong baroclinic circular vortex near the periphery of core region of a tropical cyclone. It has strong inflow in the boundary layer and outflow at the upper levels. Its stability is almost moist neutral. This stability may be too large as compared to the actual stability at this radius. However, the analysis results are not sensitive to a small reduction of stability. The field at 400 km radius approximately describes the outer region of a storm.

Table 2 shows the values used for the temperature T, the azimuthal flow V, and the other parameters derived from them at the two radii. This table indicates the pressure levels where each quantity is defined. The principal quantities are specified by taking into consideration the results of observational analyses and of numerical simulation experiments (e.g., Jordan, 1958; Kurihara, 1975). Some of the procedures used in determining the radial-vertical flow, U and W, are explained in Appendix B.

The vertical variations of Θ, V and U are obtained by the finite-differencing technique. The radial change of Θ is derived as follows. First, the radial gradient of pressure, i.e., $\partial\Phi/\partial r$, above 900 mb is estimated for the given V by applying the gradient wind balance relation. The Coriolis parameter f takes the value 5×10^{-5} s^{-1}. The pressure gradient at 1000 mb is set equal to that at 900 mb. Then, the gradient $\partial\Theta/\partial r$

TABLE 1. Pressure levels where the perturbation variables are defined.

Variable	Levels (mb)
θ	200, 400, 600, 800, 1000
u	100, 300, 500, 700, 900, 1000
v	100, 300, 500, 700, 900, 1000
ϕ	100, 300, 500, 700, 900, 1000
ω	200, 400, 600, 800, 1000

TABLE 2. Basic fields at the 150 km and the 400 km radii.

R (km)	p (mb)	T (K)	Θ (K)	$\frac{\partial\Theta}{\partial r}$ (K m^{-1})	$\frac{\partial\Theta}{\partial p}$ (K Pa^{-1})	$\frac{\partial\Phi}{\partial r}$ (m s^{-2})	V (m s^{-1})	$\frac{\partial V}{\partial r}$ (s^{-1})	$\frac{\partial V}{\partial p}$ (m s^{-1} Pa^{-1})	U (m s^{-1})	$\frac{\partial U}{\partial r}$ (s^{-1})	$\frac{\partial U}{\partial p}$ (m s^{-1} Pa^{-1})	W (Pa s^{-1})
				$\times10^{-5}$	$\times10^{-4}$	$\times10^{-3}$		$\times10^{-4}$	$\times10^{-3}$		$\times10^{-4}$	$\times10^{-3}$	$\times10^{-1}$
150	100					0.31	4.0	−0.19		1.37	−0.06		
	200	225.7	357.47	−1.53	−7.56				0.75			−0.03	−1.50
	300					3.36	19.0	−0.89		0.68	−0.03		
	400	263.5	342.36	−3.09	−8.22				0.48			−0.03	−1.78
	500					6.84	28.5	−1.33		0.0	0.0		
	600	280.5	324.58	−1.62	−8.00				0.15			−0.03	−1.78
	700					8.19	31.5	−1.47		−0.68	0.03		
	800	291.2	310.37	−0.35	−6.34				0.03			−0.03	−1.50
	900					8.43	32.0	−1.49		−1.37	0.06		
	1000	299.2	299.20	0.0	−5.59	8.43	20.2	−0.78	−1.18	−16.64	0.77	−1.53	0.0
400	100					−0.07	−1.4	−0.00		0.43	−0.01		
	200	218.0	345.27	−0.06	−6.66				0.13			−0.01	−0.20
	300					0.06	1.1	−0.02		0.21	−0.00		
	400	255.5	331.96	−0.40	−6.88				0.32			−0.01	−0.24
	500					0.51	7.4	−0.13		0.0	0.0		
	600	274.6	317.75	−0.30	−6.30				0.14			−0.01	−0.24
	700					0.76	10.1	−0.18		−0.21	0.00		
	800	287.8	306.75	−0.55	−4.64				0.17			−0.01	−0.20
	900					1.13	13.5	−0.24		−0.43	0.01		
	1000	299.2	299.20	0.0	−3.77	1.13	9.9	−0.14	−0.36	−5.2	0.08	−0.48	0.0

is obtained through the hydrostatic relation. At 1000 mb, $\partial\Theta/\partial r=0$ is assumed. In order to specify the radial change of V, the empirical relation (e.g., Riehl and Malkus, 1961)

$$V(r)=V(R)\left(\frac{R}{r}\right)^{\lambda} \tag{2.9}$$

is used, which results in $\partial V/\partial r=-\lambda V/R$ at $r=R$. As for the value of λ, Riehl and Malkus (1961) summarized that the range 0.5–0.6 appears excellent for the observed surface wind. In the present study, the surface wind is related to the wind at 900 mb and λ for the surface wind is obtained to be 0.58 if λ for the 900 mb level is set to 0.7 (Appendix B). The value 0.7 is adopted for λ at all levels above the 900 mb surface, except for the 100 mb level at the 400 km radius where $\lambda=-0.1$. Note that the relative vorticity, which is given by $(\partial V/\partial r)+(V/R)=V(1-\lambda)/R$, is positive when $V>0$ and $\lambda<1$. As for the determination of $\partial V/\partial r$ at 1000 mb and $\partial U/\partial r$ at all levels, and the subsequent computation of W, see the explanation in Appendix B.

3. Method of analysis and classification of spiral bands

a. Analysis level

The behavior of a spiral band is subject to various physical factors such as the stratification, the state of basic flow, the effect of heating, and so on. In the present study, the contribution of each factor to the intensification of a spiral band is investigated by taking the different effects, one by one, into the system of equations. The eigenvalues and the corresponding eigensolutions are obtained at each analysis level, beginning with the simplest condition and ending with the case where all terms of the prognostic equations (2.1), (2.2), (2.3) and (2.6) are involved.

In Table 3, the analysis levels are defined in ascending order by indicating the physical factor which is

TABLE 3. Definition of analysis levels. Physical factors and the corresponding terms in the prognostic equations to be added at each level are listed. The continuity equation and hydrostatic relation are used at all levels.

Analysis level	Additional factor at each level	Terms added in the prognostic equations $\frac{\partial u}{\partial t}=$	$\frac{\partial v}{\partial t}=$	$\frac{\partial\theta}{\partial t}=$	$\frac{\partial\phi_s}{\partial t}=$
AL0		$-\frac{\partial\phi}{\partial r}$	$-\frac{\partial\phi}{R\partial\varphi}$		$+\frac{1}{\rho_0}\omega_s$
AL1	static stability			$-\frac{\partial\Theta}{\partial p}\omega$	
AL2	rotation	$+fv$	$-fu$		
AL3	azimuthal flow with vertical shear	$-V\frac{\partial u}{R\partial\varphi}$ $+\frac{2V}{R}v$	$-V\frac{\partial v}{R\partial\varphi}$ $-\frac{2V}{R}u$ $-\frac{\partial V}{\partial p}\omega$	$-V\frac{\partial\theta}{R\partial\varphi}$ $-\frac{\partial\Theta}{\partial r}u$	$-V\frac{\partial\phi_s}{R\partial\varphi}$ $-\frac{\partial\Phi_s}{\partial r}u$
AL4	horizontal shear		$\left(-\frac{\partial V}{\partial r}+\frac{V}{R}\right)u$		
AL5	radial-vertical circulation	$-U\frac{\partial u}{\partial r}$ $-\frac{\partial U}{\partial r}u$ $-\frac{\partial U}{\partial p}\omega$ $-W\frac{\partial u}{\partial p}$	$-U\frac{\partial v}{\partial r}$ $-\frac{U}{R}v$ $-W\frac{\partial v}{\partial p}$	$-U\frac{\partial\theta}{\partial r}$ $-W\frac{\partial\theta}{\partial p}$	$-U\frac{\partial\phi_s}{\partial r}$
AL6	surface friction	$+\nu F_u$	$+\nu F_v$		
AL7	lateral diffusion	$+\kappa F_u$	$+\kappa F_v$	$+\kappa F_\theta$	
AL8	heating			$+q$	

to be added at each analysis level and the terms representing its effect in the prognostic equations. The continuity equation and the hydrostatic relation are applied at all analysis levels. Brief remarks on each analysis level follow:

AL0 (analysis level 0): A spiral band is in the simplest environment, i.e., a calm, neutral atmosphere without including the effects of viscosity, heating, or that of the earth's rotation. Only pure external gravity waves exist at this analysis level.

AL1: The stratification is introduced. It is almost moist neutral when $R=150$ km and near the mean condition for the tropics in the hurricane season if $R=400$ km. In addition to the external gravity waves, pure internal gravity waves appear.

AL2: The effect of the earth's rotation is taken into consideration. The waves at AL1 are modified to become neutral external and internal gravity-inertia waves. Besides these waves, the fields of almost geostrophic mode are possible. All analysis results in the following sections are for the case $f=5\times10^{-5}$ s^{-1}. Analysis is also made with $f=-5\times10^{-5}$ s^{-1} which represents the tropics of the Southern Hemisphere. The results for the latter case is briefly mentioned in Section 8.

AL3: Basic azimuthal flow V with vertical shear only is introduced. Note that the parameter $2V/R$, which appears at this level in Table 3, represents the relative vorticity for this flow. The radial variation of the basic temperature and pressure fields, which satisfies the gradient wind and hydrostatic relations, is also included.

AL4: Radial shear, $-r\partial(V/r)/\partial r$, is included in the basic flow field.

AL5: The radial-vertical circulation, i.e., U and W, is added to the basic field.

AL6: At this analysis level, the surface friction is allowed to influence the perturbation flow u and v. In the present study, the effect of vertical diffusion of u and v is assumed to be negligible except at the 1000 mb level where it is expressed by

$$_{V}F_{u}=-c_0u, \qquad _{V}F_{v}=-c_0v. \tag{3.1}$$

The value 10^{-5} s^{-1} is used for c_0.

AL7: The terms representing the effect of horizontal diffusion of u, v and θ are incorporated into the system of equations. As mentioned in Section 2a, the effect of differential azimuthal advection, which will be explained below, is considered in addition to the conventional diffusion. A constant-phase line of the spiral band makes the orientation angle B, given by (2.8), relative to the basic azimuthal flow. If the angular velocity varies with radial distance, the phase line tends to be twisted, unless $B=0$, so that the specified spiral patterns is effectively destroyed. We assume that such an effect of differential advection may be expressed in the form

$$-d\left|\frac{\partial}{\partial r}\left(\frac{V}{r}\right)\right||\sin B|\left|\frac{\partial x}{\partial \varphi}\right|, \tag{3.2}$$

where x stands for one of u, v and θ, and $d=10$ km. Then defining K_2 as the product of d, $|\partial(V/r)/\partial r|$ and $|\sin B|$, the terms for the horizontal diffusion may be written

$$\left.\begin{aligned} {}_{H}F_{u}&=K_1\left(\nabla^2u-\frac{u}{R^2}-\frac{2}{R^2}\frac{\partial v}{\partial \varphi}\right)-K_2\left|\frac{\partial u}{\partial \varphi}\right| \\ {}_{H}F_{v}&=K_1\left(\nabla^2v-\frac{v}{R^2}+\frac{2}{R^2}\frac{\partial u}{\partial \varphi}\right)-K_2\left|\frac{\partial v}{\partial \varphi}\right| \\ {}_{H}F_{\theta}&=K_1\nabla^2\theta-K_2\left|\frac{\partial \theta}{\partial \varphi}\right| \end{aligned}\right\}, \tag{3.3}$$

where $\nabla^2=-[(2\pi/D)^2+(m^2-0.25)/R^2]$ owing to (2.7) and $K_1=10^3$ m^2 s^{-1} is used.

AL8: By adding the effect of heating associated with the perturbation flow, the system of equations becomes complete. Heating of the so-called CISK type (e.g., Yamasaki, 1969) is used in this study; namely

$$q=-\omega_T\left(-\frac{\partial \Theta}{\partial p}\right)h, \tag{3.4}$$

where ω_T is the average of ω at the 800 and 1000 mb levels. For the parameter $h(p)$, two different sets of values are assigned according to the frequency of ω_T. It is assumed that, if the frequency is high, the release of latent heat is limited to the lower levels since the energy supply to convective cells does not last long. On the other hand, if ω_T varies slowly with time, deep convection may develop. Depending on $|\sigma_r|$ at the analysis level AL7, the following values are used:

h at 200, 400, 600 and 800 mb

$$=\begin{cases} 0.1,\ 0.6,\ 1.9 \text{ and } 1.8, \text{ for } |\sigma_r|\geqslant 10^{-4}\ \text{s}^{-1} \\ 1.1,\ 1.3,\ 1.2 \text{ and } 1.1, \text{ for } |\sigma_r|<10^{-4}\ \text{s}^{-1} \end{cases} \tag{3.5}$$

b. Three basic modes of spiral bands

In the previous section it was noted that, for the present vertical resolution (Table 1), the numerical solution of the perturbation equations for given m, D, and a specified type is obtained for each of 18 eigenvalues. At the low order analysis level, however, the number of meaningful solution is reduced due to the simplicity of the system. The number is 2 and 12, respectively, at AL0 and AL1. It becomes 18 at AL2. After that, each of the 18 solutions is modified as the analysis level is raised. It is not difficult to follow each solution from one analysis level to the next and,

hence, to find out how it is changed by the physical factor added at the higher level.

For the sake of convenience in the following analysis, the 18 solutions are classified into the three basic modes, each having unique characteristics at the low-order analysis level and responding to a certain physical factor quite differently at the high-order analysis level.

All solutions obtained at AL1, i.e., the spiral bands in the stratified atmosphere, are gravity wave modes. Two of them are external mode solutions and can be traced back to AL0, and the rest are pure internal mode solutions. These gravity wave modes are necessarily neutral for the present stably stratified atmosphere. (Although the computed growth rate σ_i is not exactly zero, it is very small; i.e., the computed e-folding time is 30 to 300 years, suggesting a high degree of accuracy in the numerical results.) The 12 solutions at AL1 are classified into two groups based on the direction of the radial phase velocity. The six bands which propagate radially outward are called the G-mode spiral bands. These bands are represented by a positive frequency ($\sigma_r>0$) for the N-type spirals and $\sigma_r<0$ for the S-type spirals. On the other hand, the inward propagating bands, for which the sign of the frequency is opposite to that mentioned above, are defined as the H-mode spiral bands.

The above-mentioned neutral gravity waves, propagating in a cylindrical coordinate domain, bring about the radial transport of energy through the so-called pressure work. Accordingly, a small central area is a region of energy source or sink for these waves.

Fig. 2 is presented to illustrate the structure of each of the six N-type G-mode bands at AL1, which are denoted by the symbols G1, G2, etc. This figure represents the case for $m=2$ and $D=200$ km. Later, it will turn out that this case yields the most unstable band of the G-modes. In Fig. 2, the schematic flow pattern and the temperature perturbation on the radial vertical cross section are shown as well as the distributions of u and ω on the verticals along which they vary the most. All flow patterns for G1–G6 do not exhibit vertical tilt. The values of u and ω in the figure are normalized with respect to the maximum u. These variables have the units m s^{-1} and 10^{-2} mb s^{-1}, respectively.

The vertical velocity w is related to ω by

$$\omega=\frac{\partial p}{\partial t}+\mathbf{V}\cdot\nabla p+w\frac{\partial p}{\partial z}.$$

Using the hydrostatic balance relation, w is given by

$$w=\left(\frac{\partial\phi}{\partial t}+\mathbf{V}\cdot\nabla\phi-\frac{\omega}{\rho}\right)\frac{1}{g},$$

where ρ is the density of air and g the gravitational acceleration. Note that the tendency equation (2.3) is the linearized version of this equation under the condition $w=0$. Usually, w is approximated by $-\omega/(\rho g)$ except near the surface where the contribution from $(\partial\phi/\partial t+\mathbf{V}\cdot\nabla\phi)/g$ is not negligible. The above rule applies to the internal gravity wave modes G2–G6. For the external gravity wave mode G1, the two terms $\partial\phi/\partial t$ and $-\omega/\rho$ more or less cancel and w becomes very small at all levels. If w of this mode is computed at AL0 by using the density corresponding to the isothermal air, it vanishes everywhere and the Lamb wave is obtained.

In Fig. 2, the radial variation of the surface pressure p_s is shown by the dotted lines. This variation is derived from the geopotential height of the 1000 mb surface. For the same maximum amplitude of u, the amplitude of p_s increases as the number of nodal points in the vertical profile of u or ω decreases. The phase speed of outward propagation is estimated by $\sigma_r D/(2\pi)$ and is also shown in the figure. Except for G6, the frequency σ_r is very large compared to f, suggesting the insensitivity of frequency for G1–G5 to the effect of the earth's rotation. The field of v (not shown in Fig. 2) has an interesting feature. For the G1–G5 modes, the correlation between v and u is positive for the N-type spiral while it is negative for the S-type. In other words, the angular momentum is transported outward by the N-type spiral and inward by the S-type. This suggests that, when the horizontal shear of basic flow is incorporated at AL4, either the N-type or the S-type spiral will respond positively to the shear and the spiral of the other type may be damped.

The H-mode spiral bands at AL1, i.e., H1, H2, etc., are quite similar to the corresponding G1, G2, etc., except for the 180° phase difference of the thermodynamical field and the reverse in the direction of radial propagation. The correlation between u and v is the same with that for the G-mode. It will be shown later that the H-mode bands are sensitive to heating and their behavior becomes different from that of the G-modes.

At AL2, when the Coriolis term is included in the momentum equations, six more solutions appear besides the G-mode and H-mode bands. They will be called the F-mode spiral bands. At this analysis level, however, the growth rate of the F-mode bands are nearly zero and the obtained perturbation flows are almost geostrophic. At AL3, when the basic axisymmetric wind with the vertical shear is introduced, the bands are advected and a weak dynamical coupling between the neighboring levels occurs through a very weak vertical motion. Fig. 3 shows the vertical variations of the amplitude and phase of u, v for F1 through F6 (N-type). It is seen that the amplitude of an F-mode band is predominant at a certain pressure level and the phase difference between u and v is

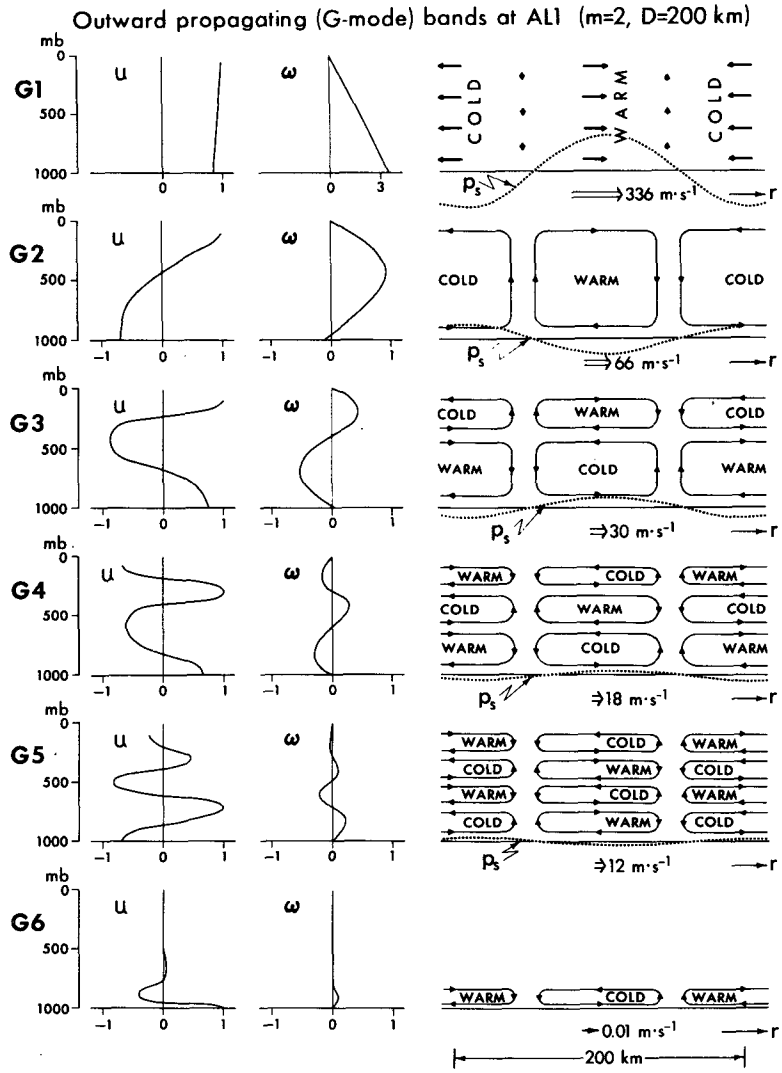

FIG. 2. Structure of N-type G-mode bands at AL1. The parameters are specified as $m=2$ and $D=200$ km. Vertical profiles of u and ω, schematic flow patterns and perturbation temperature fields for the radial-vertical cross section, radial variation of surface pressure (dotted line), and the radial speed of phase propagation are shown for modes G1 through G6.

about 180°. In the case of S-type F-modes, v is almost in phase with u. This may imply that either of the N-type or the S-type F-mode band is selectively amplified in the presence of the horizontal shear of the basic flow.

It should be mentioned here that there are 36 solutions for a set of scale parameters m and D, i.e., 18 solutions each for N-type and S-type. In this subsection, the solutions were classified into three basic modes according to their dynamical features. Now, the bands of N-type G-mode, N-type H-mode, and N-type F-mode can be paired with those of S-type H-mode, S-type G-mode, and S-type F-mode, respectively. These matches can be made from inspection of the obtained solutions particularly at the low-order analysis levels. For example, the N-type G3-mode and the S-type H3-mode constitute a pair of complex conjugate solutions at AL3. They have the same frequency (σ_r), and the amplifying rate (σ_i) of the former band and the damping rate ($-\sigma_i$) of the latter band are the same. A similar comparison of the growth rates of paired bands may be made by using the figures to be presented later (Figs. 5, 8 and 10). For instance, the growth rates of N-type G-mode bands at AL3 or AL4 can be compared with those of the S-type H-modes; also the growth rates for the N-type F-modes can be compared with those of the S-type F-modes. Usually, a damping component is not of interest in the investigation of instability. However, in the present study, all bands are traced

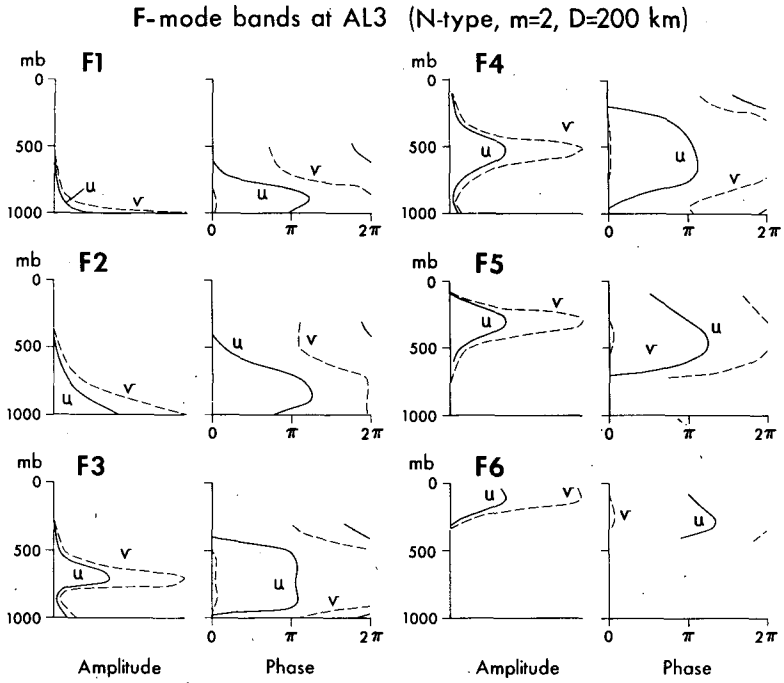

FIG. 3. Structure of N-type F-mode bands at AL3. The parameters $m=2$ and $D=200$ km are used. The amplitude and phase of u and v as a function of pressure level are shown for modes F1 through F6.

to the higher order analysis levels in order to see the effect of various physical factors on the behavior of the bands. In the following sections, this discussion is presented separately for each mode.

4. Development of G-mode bands

Instability of the G-mode bands in the inner region of a tropical cyclone ($R=150$ km) is investigated first. The growth rates of each G-mode were obtained at all analysis levels for different wavenumbers ($m=0$ through $m=6$ and both N-type and S-type spirals) and different radial scale ($D=10$ through 400 km). According to the present calculations, the most unstable band at AL8 is the N-type G3-mode spiral with $m=2$ and $D=200$ km. The growth rate of this band is 4.16×10^{-5} s^{-1}, or its e-folding time is 6.7 h. Fig. 4 shows the growth rate of the G3-mode band at AL8 as a function of m and D. It is seen that the N-type pattern has large growth rates, with wavenumbers $m=1$ to $m=3$ being preferred for development while the S-type pattern has a large damping rate for all wavenumbers greater than $m=1$. The preferred radial scale is 200 km, corresponding to a band width of 100 km. In Fig. 4, the neutral stability curve for AL7, i.e., the adiabatic case, is shown by a heavy dashed line. It is seen that the area of instability is larger for AL8 than for AL7, but not by very much. It may be suggested that the preferred shape and scale of the spiral pattern of the G3-mode band are changed little by the effect of heating.

In order to see the effects of different physical factors on the stability of the G-mode bands, the variation of the growth rate with the analysis levels is examined for each mode. The parameters m and D are fixed at 2 and 200 km, respectively. The analysis results are presented in Fig. 5 in a form of a column diagram. In case of the N-type spiral, all modes are neutral at AL1 and AL2. The baroclinicity which is introduced at AL3 does not have a significant effect on any mode. The external gravity wave mode G1 is excited at AL4 but is suppressed at AL5 when the basic circulation on the radial-vertical plane is introduced. The growth rates of the internal gravity wave modes (G2, G3, G4) increase significantly at AL4 and AL8. This result indicates the positive contribution of horizontal shear of the basic azimuthal flow and also of the heating effect to the development of the spiral band. Note that the modes G2, G3 and G4 can develop even in the adiabatic case. Accordingly, the heating effect appears not to be the factor of the primary importance. The energetics of the G3-mode band at AL8 is given in Section 7. In the present case, the mode G5 develops at AL4 but it is stabilized by the effect of heating. The G6-mode does not develop at any analysis level. The unstable bands at AL8, i.e., G2, G3 and G4, propagate outward and counterclockwise. Their radial phase speeds are 69, 33 and 25 m s^{-1}, respectively.

As for the S-type spirals, all G-mode bands except G6 cannot develop as seen in Fig. 5. The S-type G6 is

excited at AL5 when the radial and the vertical component of basic flow are incorporated. Every G-mode band, both N-type and S-type, propagates radially outward at AL2. Most of them still move outward at AL8, although the speed is affected by the physical factors added at the higher analysis levels. However, in case of the S-type G6-mode band, even the moving direction is changed and it propagates inward at a speed of 31 m s^{-1}.

The stability of the spiral bands in the outer region of the storm was also analyzed by applying the basic field specified for the 400 km radial distance (Table 2). The computed values of the growth rate indicate that, when the diffusion effects are included, no G-mode bands of any spiral shape develop significantly in the outer region. Some bands have a large damping rate and others are almost neutral. For example, the growth rate of the G3-band with $m=2$ and $D=200$ km at AL7 is -0.03×10^{-5} s^{-1} for the N-type spiral and -0.35×10^{-5} s^{-1} for the S-type. Adding the effects of heating at AL8, the growth rates for those bands become slightly positive, i.e., the corresponding e-folding times are 81 and 230 h, respectively, for the N-type and S-type bands. However, these growth rates are insignificant for the fast moving bands.

Based on the analysis results obtained so far, it may be speculated that the N-type G3-mode spiral band with $m=2$ and $D=200$ km develops in the inner area of a tropical cyclone, propagates outward, and becomes neutral in the outer region. In order to see the smooth transition of the band structure between the inner and the outer area, Fig. 6 is presented. In this figure, the radial-vertical cross sections of u, ω, v, ϕ and θ at $R=150$ km at AL8 and those at $R=400$ km at AL7 are compared. At $R=400$ km, AL7 is chosen in assuming that the air is not quite moist. At any rate, the behaviors of the band at AL7 and AL8 are about the same in the outer region. The similarity between the corresponding fields in the left and the right parts of the figure is very good. The radial (outward) phase speeds at the two radii are nearly the same—33 m s^{-1} at 150 km and 26 m s^{-1} at 400 km. Accordingly, the gradual transformation of the band during its outward propagation seems to be probable. The cross sections of u and ϕ at both $R=150$ km and $R=400$ km clearly shows the positive correlation between the two variables. Therefore, the energy of the band is transported outward through the pressure work.

Kurihara and Tuleya (1974) made a detailed analysis of the bands which appeared in the outer area of a three-dimensional numerical simulation model of a tropical cyclone. Tuleya and Kurihara (1975) examined the role of asymmetric structure in the energetics

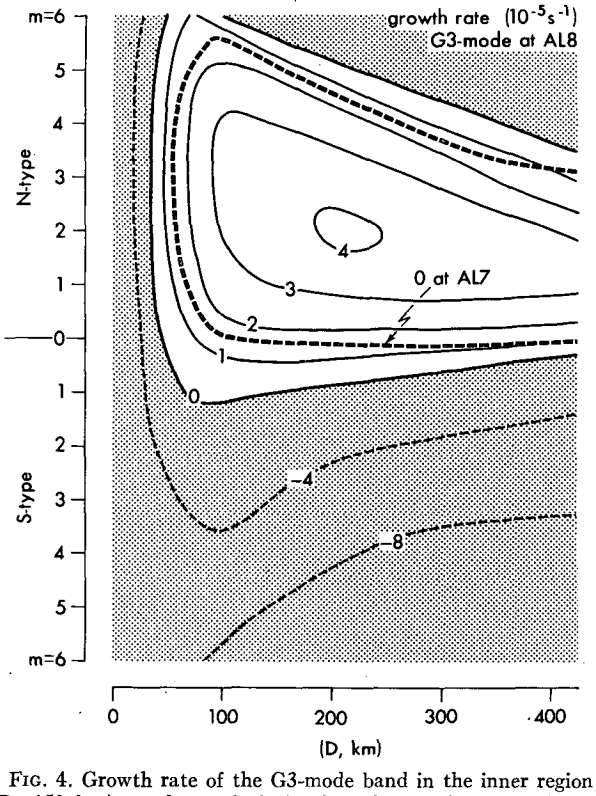

FIG. 4. Growth rate of the G3-mode band in the inner region ($R=150$ km) at the analysis level AL8 as a function of the wavenumber m and the radial scale D. The negative region is shaded. Heavy dotted line is the neutral stability curve at AL7.

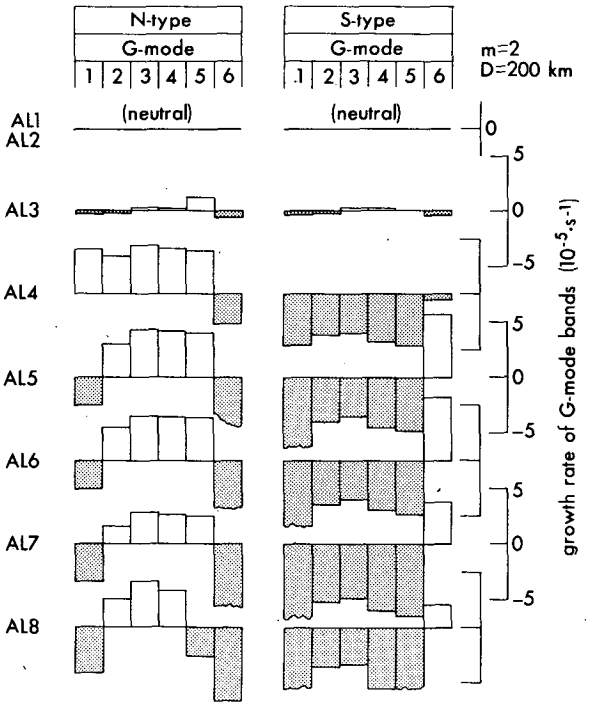

FIG. 5. Instability of the G-mode bands ($m=2$, $D=200$ km) at the different analysis levels. The growth rate for each of the modes G1 through G6, both N-type and S-type, is represented by the height of the column. A stable damping mode is indicated by a shaded column extending below the horizontal neutral line.

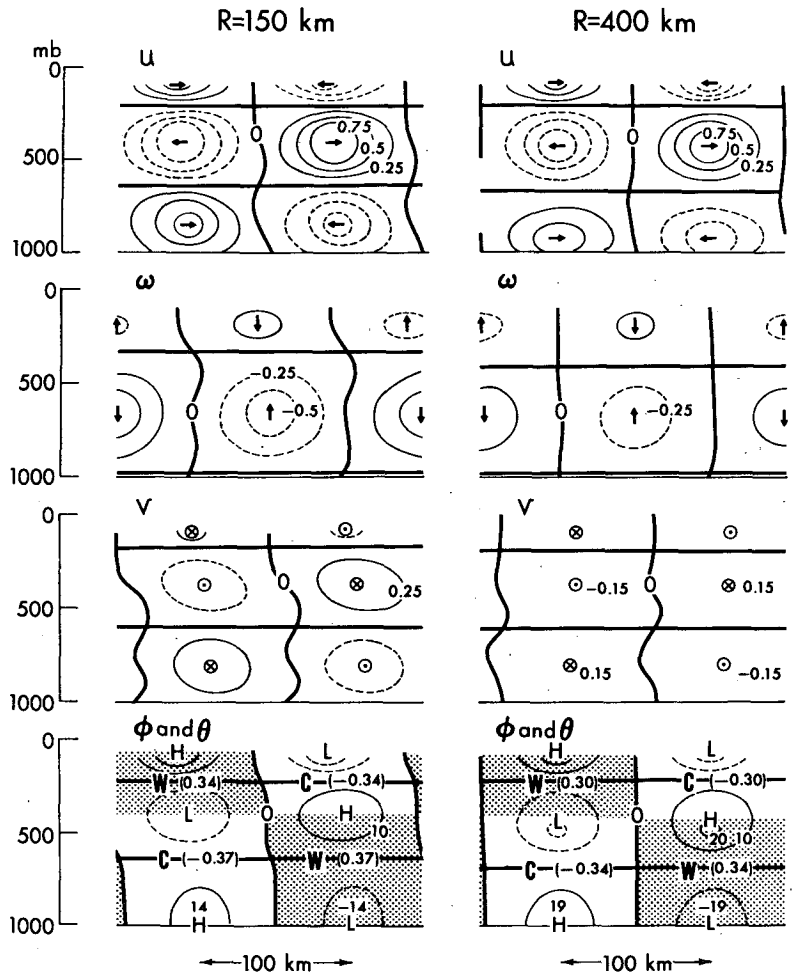

FIG. 6. Structure of the G3-mode band ($m=2$, $D=200$ km) at $R=150$ km at AL8 and at $R=400$ km at AL7. Radial-vertical cross sections of u, ω, v, ϕ and θ are presented. Shaded areas in the lower cross sections show warm regions in the θ perturbation.

of the above model. From the comparison of their results with the present analysis, it may be concluded that the band which developed in their model corresponds to the N-type G3-mode band. Kurihara (1975) noticed that an outward propagating band also appeared in his axisymmetric model. This may be a manifestation of the weak instability of the band with $m=0$ as shown in Fig. 4.

The structure and behavior of the so-called outer spiral bands in a real tropical cyclone can be described fairly well by those obtained in the above-mentioned three-dimensional models (Kurihara and Tuleya, 1974). Thus, the actual outer spiral bands, at least some of them, may be interpreted as the counterclockwise, outward-propagating, internal gravity-inertia waves which are intensified in an inner area by the radial shear of the azimuthal flow and possibly also by the effect of heating.

5. Development of H-mode bands

The H-mode spiral bands are defined as the inward propagating gravity waves at AL1. The analysis of these bands in the inner area ($R=150$ km) revealed that the H3-mode band responds strongly to heating. Fig. 7 shows the distribution of the growth rate of H3-mode at AL8 in the wavenumber and radial scale domain. The neutral stability curve for the same mode in the adiabatic case (AL7) is also shown. In the absence of heating, the instability is limited to the N-type spirals only and for the parameter range $m=1$ to $m=4$ and $D\gtrsim 100$ km. The unstable region outside the heavy dashed curve in Fig. 7 is established by the heating effect at AL8. The growth rate of the S-type spiral with radial scale in the order of 10 km is especially large. It exceeds 2×10^{-4} s^{-1}, or the e-folding time is in the order of 1 h.

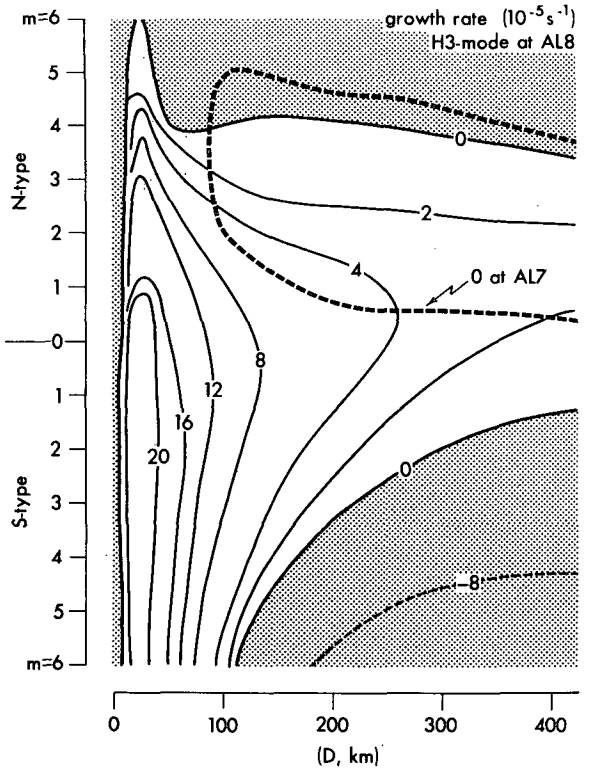

FIG. 7. As in Fig. 4 except for the H3-mode band.

The dynamical response of each of the H-mode bands is presented in Fig. 8 for the case $m=2$ and $D=200$ km which represents a case favorable for the instability without heating. This figure, which is similar to Fig. 5, shows the growth rates of each mode at the different analysis levels. In the case of the N-type spirals, the H1–H5 modes are destabilized by horizontal shear of the basic azimuthal wind. However, only the H2 and H3 modes remain unstable at AL8. Their radial phase velocities at AL8 are directed inward and have the values 54 and 14 m s^{-1}, respectively. It is seen that the radial and vertical flow introduced at AL5 acts to suppress the external gravity wave mode H1 as well as the H4 and H5 modes. As seen in Fig. 8, the latter modes are further stabilized by the effect of heating. All S-type modes with $m=2$ and $D=200$ km are dynamically stable at the analysis level AL7. The S-type H3-mode with this scale is excited by the heating at AL8 and propagates inward with a phase speed of 31 m s^{-1}.

As suggested by Fig. 7, the spiral bands, both N-type and S-type, with a radial scale <75 km may grow in the inner area if the heating effect as parameterized in the present study is added. In that case, the H3-mode, especially that with S-type pattern, is sensitive to the heating effect. All of the thermally excited bands propagate inward. The speeds of S-type H3-mode spirals ($m=2$) with $D=25$ km and $D=50$ km are 19 and 21 m s^{-1}, respectively.

The instability analysis was carried out also for the H-mode bands in the outer region of a storm. There exists no H-mode band which is dynamically unstable at AL7. The addition of the heating effect does not destabilize it. For example, the growth rate of the H3-mode with $m=2$ and $D=200$ km at AL8 is -0.23×10^{-5} s^{-1} for the N-type and -0.43×10^{-5} s^{-1} for the S-type, respectively. The corresponding values for $D=100$ km are -0.58×10^{-5} s^{-1} and -0.67×10^{-5} s^{-1}, respectively, indicating a larger damping rate for a band with a smaller radial scale.

As H-mode spirals propagate inward and they may grow only in the inner region, these spirals, if observable, would appear in the inner area only. However, spirals of this kind have not been definitely observed in a real storm. This should be either due to modeling problems which might have yielded fictitious solutions or due to some factors which may deform the idealized solutions. In the present study, the effect of heating is incorporated at AL8 through Eq. (3.4). Contribution of this effect in comparison to the adiabatic warming or cooling effect due to local vertical motion depends on the phase relation between the local ω and ω_T as well as on the parameter h. Accordingly, some modes having a favorable distribution of ω at a certain radius may respond to

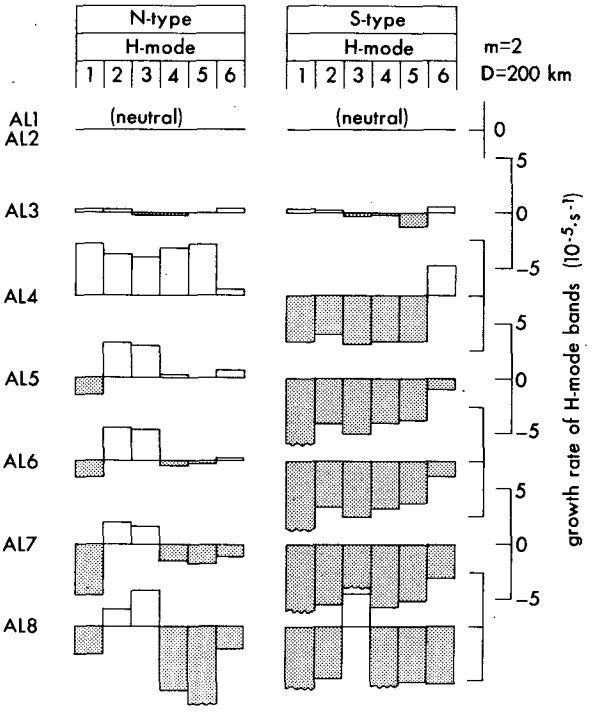

FIG. 8. As in Fig. 5 except for the H-mode bands ($m=2$, $D=200$ km).

heating more strongly than others. The scheme (3.4) is applied regardless of the sign of ω_T, i.e., the heating effect is considered as unconditional. It is difficult to assess the degree of validity of the above scheme and hence the accuracy of the H-mode solutions with small radial scale. Even if the accuracy is tolerable, the solutions may be too idealistic. For the narrow H-mode bands to develop, sufficient moisture in the boundary layer is required. If the moisture content is not uniform, the bands may appear sporadically. Addition of nonlinear effects may also deform the solutions of a linearized system.

6. Development of F-mode bands

It was mentioned in Section 3 that the appearance of the F-mode bands at a low-order analysis level is associated with the Coriolis force and each band has a predominant amplitude at a certain level only. The analysis of F-mode bands at higher analysis levels showed that the most unstable F-mode in the inner area of a tropical cyclone is the F3-mode with S-type pattern. Fig. 9 shows the growth rate of the F3-mode at AL8 as a function of wavenumber and radial scale. The neutral stability curve at AL7 is also drawn. The dynamical instability of the S-type spirals is clearly indicated. This is in contrast to the case of the gravity wave modes, i.e., the G-modes and H-modes, for which the N-type pattern is dynamically unstable. As suggested in Section 3, selection of an unstable spiral pattern in the presence of the radial shear of the basic flow is apparently related to the transport of angular momentum. All the dynamically unstable bands, i.e., N-type G-mode, N-type H-mode and S-type F-mode, transport the angular momentum radially outward. The maximum growth rate of the F3-mode at AL8 is found at $m=2$ and $D=300$ km. However, as mentioned before, the accuracy of solution is lowered for a larger value of D. The slight difference in the size of the unstable domain between AL7 and AL8 suggests that there is little effect of heating on the F3-mode.

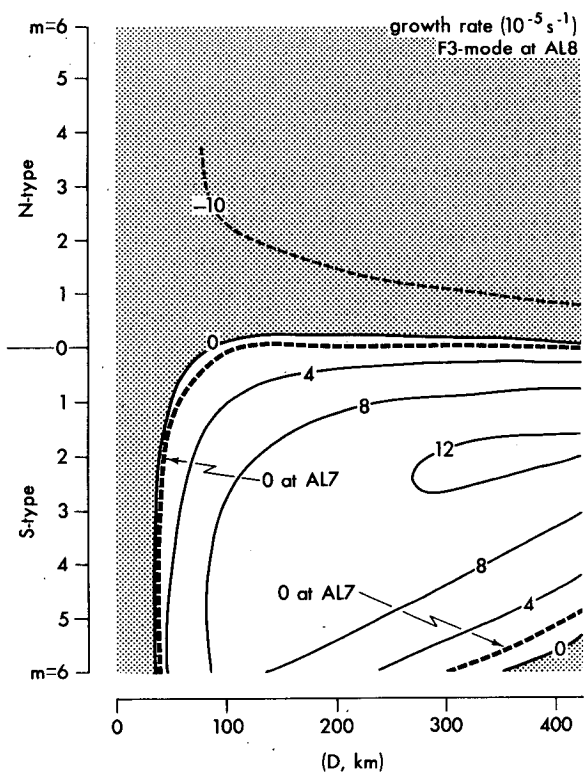

FIG. 9. As in Fig. 4 except for the F3-mode band.

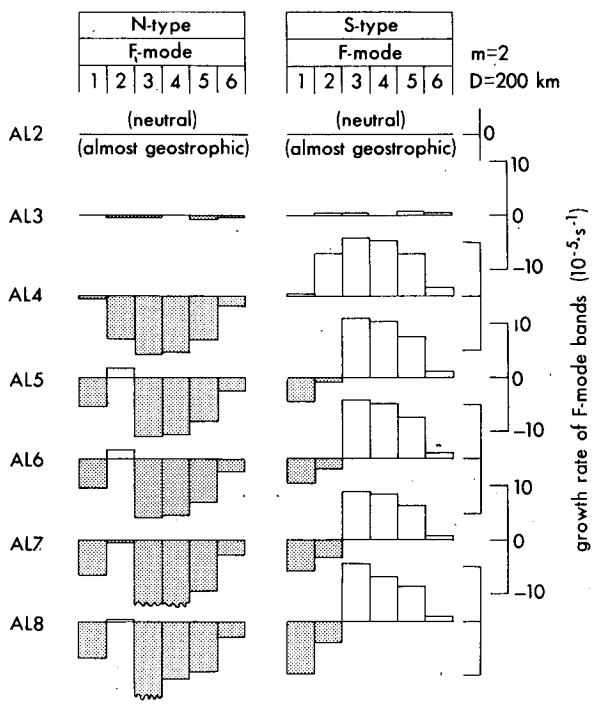

FIG. 10. As in Fig. 5 except for the F-mode bands.

The variation in growth rate of the F-mode bands with the analysis level is presented in Fig. 10 for the case $m=2$ and $D=200$ km. It is evident from this figure that the N-type pattern is stable for all F-mode bands except F2 which is nearly neutral. On the other hand, the S-type spiral is unstable for the three modes, F3, F4 and F5. The growth rate for these modes increases when the horizontal shear of the basic azimuthal flow are taken into consideration at AL4. Their phase propagation at AL8 is directed radially inward (14, 12 and 7 m s^{-1} for the F3, F4 and F5 bands, respectively) and counterclockwise (32, 31 and 27 m s^{-1}, respectively). The azimuthal movement may be compared to the azimuthal component of the basic flow at the level where each mode has the maximum amplitude. It is 32 m s^{-1} at 700 mb for the case of F3, 29 m s^{-1} at 500 mb for F4, and 19 m s^{-1} at 300 mb for F5. Accordingly, the unstable F-mode bands ap-

pear to move in the azimuthal direction with a phase velocity close to that of the basic flow. Two other F-modes (F1 and F2) which show the largest amplitude at the surface at AL4 are suppressed at AL5 by the basic radial wind. The growth rate of the F6-mode is positive but relatively small at all analysis levels after AL4, as shown in the figure.

The behavior of F-mode bands in the outer region ($R=400$ km) was also investigated. The N-type F-mode cannot develop at all. For some modes of the S-type spiral, the growth rates are slightly positive. For instance, the e-folding time for the most unstable mode, which is F3, is 63 h at AL7 and 53 h at AL8.

According to the present analysis, the F-mode bands may appear in the inner area of a storm, although the detection may not be easy because they grow in the free atmosphere and have small vertical extent. The F-mode bands have never been reported in actual observations.

7. Energetics of the unstable spiral bands

a. Energy budget equations

The energetics of spiral bands is investigated by analyzing the energy budget equations which can be derived from the system of perturbation equations. In the following, square brackets are used to denote the space average of a quantity, i.e., average with respect to pressure for the range 0 to 1000 mb, with respect to azimuthal angle φ_0 to $\varphi_0+(2\pi/m)$ where φ_0 is arbitrary, and with respect to radius $R-(D/2)$ to $R+(D/2)$.

The time rate of change of the perturbation kinetic energy K_E, which is defined by $[(u^2+v^2)/2]$, is determined by

$$\frac{\partial K_E}{\partial t}=\{K_M,K_E\}_H+\{K_M,K_E\}_V +\text{generation}+\text{dissipation}. \quad (7.1)$$

The first and second terms in the right-hand side indicate the transformations from K_M (the kinetic energy of the basic flow), each being associated with the horizontal and the vertical transport of momentum, respectively. They are written as

$$\{K_M,K_E\}_H=\left[-u^2\frac{\partial U}{\partial r}-v^2\frac{U}{R}-uv\frac{\partial V}{\partial r}+uv\frac{V}{R}\right],$$

$$\{K_M,K_E\}_V=\left[-u\omega\frac{\partial U}{\partial p}-v\omega\frac{\partial V}{\partial p}\right].$$

The generation and dissipation of K_E are calculated from

$$\text{generation}=\left[-u\frac{\partial \phi}{\partial r}-v\frac{\partial \phi}{R\partial \varphi}\right],$$

$$\text{dissipation}=[u({}_HF_u+{}_VF_u)+v({}_HF_v+{}_VF_v)].$$

The available potential energy A_E is defined for the perturbation field by

$$A_E=\left[c\frac{\theta^2}{2}\right],$$

where

$$c=\frac{R_g}{p}\frac{T}{\Theta}\left(-\frac{\partial\Theta}{\partial p}\right)^{-1}.$$

The time variation of A_E depends on the energy conversion from the available potential energy of the basic state A_M, the conversion relating to the overturning process, the generation due to heating and the effect of diffusion of θ:

$$\frac{\partial A_E}{\partial t}=\{A_M,A_E\} +\text{conversion}+\text{generation}+\text{diffusion}. \quad (7.2)$$

The budget components are calculated from

$$\{A_M,A_E\}=\left[-c u\theta\frac{\partial\Theta}{\partial r}\right],$$

$$\text{conversion (overturning)}=\left[-c\omega\theta\frac{\partial\Theta}{\partial p}\right],$$

$$\text{generation}\ \{q,A_E\}=[cq\theta],$$

$$\text{diffusion}=[c\theta_H F_\theta].$$

The conversion effect is indirectly included, with the opposite sign, in the generation term in (7.1) and, hence, denotes the energy conversion from K_E to A_E, i.e., $\{K_E, A_E\}$.

The perturbation temperature T_E is defined by $T_E=\theta T/\Theta$. In the present study, the radial pressure work $u\phi$ and the radial transports of v and T_E are also computed.

b. Energetics

The energetics of the primary unstable bands in the inner area of a tropical cyclone, shown in Table 4 for the G, H and F modes, was derived from the eigensolutions at the analysis level AL8. This table also includes the energetics of a neutral G-mode band in the outer region at AL7. Note that a small radial scale is chosen for the S-type H3-mode band. A comparison of values in this table is meaningful only among the numbers in the same column. The appropriate units for each quantity is shown in the last column of the table for the sake of convenience, although the absolute magnitude of the numbers cannot be determined. The values in this table inevitably include some truncation errors which are due to the schemes used for numerical estimates.

TABLE 4. Budget of kinetic and available potential energy of spiral bands. The transports $[uv]$, $[uT_E]$ and $[u\phi]$ are also shown. Comparison of values is meaningful only among numbers in the same column. The appropriate units for each quantity is shown in the last column.

Parameters	Bands G-mode		H-mode		F-mode	Appropriate units
Position R (km)	150	400	150	150	150	
Type of spiral	N	N	N	S	S	
Wavenumber	2	2	2	2	3	
Radial scale D (km)	200	200	200	25	200	
Chosen mode	G3	G3	H3	H3	F3	
Analysis level	AL8	AL7	AL8	AL8	AL8	
K_E	4.20	2.81	0.77	0.57	2.76	10^{-1} m^2 s^{-2}
$\{K_M, K_E\}_H$	5.27	0.17	0.56	−0.52	7.83	10^{-5} m^2 s^{-3}
$\{K_M, K_E\}_V$	0.26	0.01	0.16	0.15	0.09	10^{-5} m^2 s^{-3}
Generation of K_E	−0.90	−0.10	0.32	4.98	1.09	10^{-5} m^2 s^{-3}
Dissipation of K_E	−1.12	−0.09	−0.23	−0.79	−2.10	10^{-5} m^2 s^{-3}
A_E	2.11	2.38	0.28	0.17	0.15	10^{-1} m^2 s^{-2}
$\{A_M, A_E\}$	0.36	−0.03	−0.09	−0.06	0.03	10^{-5} m^2 s^{-3}
Overturning effect	1.16	0.07	−0.18	−4.07	−1.18	10^{-5} m^2 s^{-3}
$\{q, A_E\}$	0.65	0.0	0.51	5.41	1.63	10^{-5} m^2 s^{-3}
Diffusion effect	−0.50	−0.06	−0.06	−0.22	−0.12	10^{-5} m^2 s^{-3}
Transport $[uv]$	2.29	0.86	0.46	−0.08	2.07	10^{-1} m^2 s^{-2}
Transport $[uT_E]$	0.18	0.08	−0.02	−0.02	0.08	10^{-1} K m s^{-1}
Transport $[u\phi]$	1.51	1.37	−0.17	−0.12	−0.07	10 m^3 s^{-3}

It is clearly seen from this table that the N-type G3-mode band in the inner area develops primarily through the process which transforms K_M to K_E, i.e., $\{K_M, K_E\}_H$. This process is related to the outward transport of momentum ($uv>0$) and the horizontal shear of basic flow ($-\partial V/\partial r+V/R>0$). It is noted here that the relative vorticity of the basic flow field is positive at all levels. Thus, the present basic flow field is inertially stable. The energy sources for A_E of this band are the conversion from K_E and diabatic heating to a lesser degree. The positive conversion $\{K_E, A_E\}$ is associated with the development of the θ perturbation due to the sinking of warm air and the rising of cold air. The energy sinks of K_E and A_E are small compared with the energy supply so that the instability of this band is established. This band yields an outward transport of angular momentum and internal energy.

In the outer area ($R=400$ km), the N-type G3-mode band is almost neutral as discussed in Section 4. Table 4 shows that the term $\{K_M, K_E\}$ in the K_E equation and the conversion term in the A_E equation are well balanced with the other terms of the opposite sign, respectively. The correlation $[\phi u]$ is positive, indicating the outward transport of energy by the pressure work as mentioned before.

The N-type H3-mode band with the radial scale 200 km is excited by the effects of both $\{K_M, K_E\}$ and diabatic heating. A certain amount of energy is converted from A_E to K_E.

On the other hand, the instability of the S-type H3-mode band with a small radial scale is caused by diabatic heating. The A_E is generated and becomes a main energy source for K_E. The conversion from A_E to K_E is achieved by the so-called overturning process. The term $\{K_M, K_E\}_H$ in the K_E budget takes a small negative value. The above-described energetics reflects the sensitivity of this band to the effect of heating which was analyzed in Section 5.

As for the S-type F3-mode band, it is different from the G3 and H3 bands in that the ratio of A_E to K_E is fairly small. The transformation process $\{K_M, K_E\}_H$ is the main source of K_E. This is related to the down-gradient transport of angular momentum by the S-type F-mode band in the basic circular flow. A weak conversion from A_E is the other source for K_E. The diabatic heating causes an increase of A_E for this band.

Tuleya and Kurihara (1975) investigated the energetics for their three-dimensional numerical model of a tropical cyclone. In their model, the asymmetries primarily developed through the transformation of both the kinetic energy of the axisymmetric flow and the total potential energy. They mentioned the possibility of the coexistence of two kinds of eddies, each being energetically independent of the other. The results of the energy budget analysis presented in this section support the above speculation to some degree. Namely, the process $\{K_M, K_E\}_H$ contributes to the growth of the N-type G3-mode and the S-type F3-mode bands, while the conversion of potential energy through the overturning process is responsible for the development of the S-type H3-mode band.

8. Summary and remarks

A linear stability analysis was carried out for the spiral bands in a tropical cyclone. It was revealed that three kinds of bands can be intensified in the inner area of a present model. The N-type G3 mode, the S-type H3-mode, and the S-type F3-mode are typical of these bands. The baroclinicity of a basic field is not required for the development of these spirals. The G-mode and H-mode bands are reduced to neutral gravity-inertia waves if the basic circular vortex is removed. The N-type G3-mode is an internal mode solution at this low-order analysis level. It is excited dynamically by the radial shear of basic flow and receives energy through the transformation $\{K_M, K_E\}_H$. Its preferred spiral scale is represented by wavenumber 2 and a radial scale (twice the band width) of 200 km. The S-type H3-mode is also an internal gravity-inertia wave at a simplified analysis level. Diabatic heating is responsible for its development. Its preferred radial scale is very small, about 25 km. At a low-order analysis level, the F-mode band has the form of a geostrophic mode. The vertical coupling of the F-mode bands are very weak at all levels. The major energy source for this band is the transformation $\{K_M, K_E\}_H$. This band is most unstable for wavenumber 2 and a radial scale of about 300 km.

Of the three spiral bands mentioned above, only the N-type G3-band propagates radially outward while the other two move inward. In the outer region of the storm, there exists practically no instability for a spiral of any type and mode. The N-type G3-mode band is neutral in the outer area. It is speculated that the G3-band developed in the inner area becomes a neutral wave while propagating outward. The results of the present analysis suggest a possibility that some of the observed outer spiral bands in the Northern Hemisphere may indeed be interpreted as internal gravity-inertia waves of the N-type G-mode.

The spirals corresponding to the H-mode or F-mode, which should appear in an inner area only, have never been definitely observed in a real storm. The solutions of these modes, obtained for a linearized system, may be either fictitious, or too idealistic, or difficult to detect in a real storm.

Recently, Diercks and Anthes (1975) made an analysis of the spiral band. They also investigated the dynamics of bands by dealing with an initial value problem. They concluded that the rainbands are the visual evidence of internal gravity-inertia waves in the lower troposphere. They also mentioned that the formation of bands requires neither inertial instability nor latent heat release. However, the growth of bands in an inner area in their linear analysis for the statically stable and adiabatic case was very slow. It is speculated that this is probably due to the crude vertical resolution of their linear model, which probably makes down-gradient radial transport of angular momentum above the boundary layer very small. Then, the supply of kinetic energy to the perturbation from the mean azimuthal flow would be far less compared to that in a model with better vertical resolution.

The behavior of the spiral bands in the Southern Hemisphere was investigated by changing the sign of the Coriolis parameter. The terms including the Coriolis force are, of course, directly affected. Moreover, the direction of the basic azimuthal flow, which satisfies the gradient wind relation, is reversed. The results of the analysis shows that all the arguments made for the Northern Hemisphere hold with the exchange of N-type and S-type. Accordingly, only the S-type G-mode spiral band may be observed in the outer region of a tropical cyclone in the Southern Hemisphere.

There are some factors which may play a role in the dynamics of the bands but could not be treated in this study. The Ekman layer instability is one of them. In the present study, the basic meteorological field is assumed to be axisymmetric. When the asymmetric component is included in the basic state, there may be a quadrant where the mean condition is particularly favorable for the development of a perturbation. The asymmetric basic flow may also contribute to the possible formation of the banded structures of the different kind.

It goes without saying that the movement of individual convective cells is different from the propagation of a spiral band discussed in this paper. A carefully designed mesoscale analysis, such as the analysis of the time variation in rainfall intensity or the tracing of groups of radar rain bands (e.g., Staff Members, Tokyo University, 1969), is required to reveal a mesoscale spiral structure in a tropical cyclone.

An analysis method similar to the one used in this study may be applied to the study of other meteorological phenomena. Also, it may be utilized in detecting the potential for the development of mesoscale systems in a given large-scale meteorological field.

Acknowledgments. The author would like to express his appreciation to Dr. J. Smagorinsky for the constant encouragement he has received in the present work and to Dr. K. Bryan for the discussions which stimulated him. He is indebted to Drs. Y. Hayashi and F. B. Lipps and Mr. R. E. Tuleya for many valuable suggestions to clarify and improve the interpretation and the description of the results of analysis. He also appreciates the useful comments by reviewers. A computer program to solve an eigenvalue problem was prepared based on the program kindly offered by Dr. Y. Hayashi, who obtained the original version from Dr. M. Yamasaki. Thanks are also due to Ms. E. Thompson for typing the manuscript and to Messrs. P. G. Tunison and J. N. Conner for the preparation of the figures.

APPENDIX A

Remarks on the Numerical Schemes Applied to the Perturbation Equations

It was mentioned in Section 2 that the numerical scheme for the terms involving vertical derivatives in the perturbation equations should be formulated carefully when the vertical resolution of the model is coarse.

In the present study, the hydrostatic equation is treated based on the estimate of thickness between p and $p+100$ mb, where p is a multiple of 100. The values of θ, which are defined only at 200 mb intervals as seen in Table 1, are linearly interpolated with respect to pressure to obtain values at the $p+50$ mb level ($\theta=0$ at $p=0$ mb is assumed). Multiplying θ thus interpolated with the factor

$$R_d[(p+50)/p_{00}]^{\kappa} \ln[(p+100)/p]$$

gives the thickness or the difference in ϕ between the p and $p+100$ levels.

In dealing with the continuity equation, u and v are considered to vary linearly with p between levels where they are defined.

The vertical transport of momentum in (2.1) and (2.2), i.e., $W\partial u/\partial p$, $\omega\partial U/\partial p$, etc., are estimated in the conventional manner at every 200 mb level starting at 0 mb, where they are set to equal to zero. The values thus obtained are linearly interpolated, if required, to give the value at the intermediate level where u and v are defined. To obtain the vertical transport term $W\partial\theta/\partial p$ in (2.6), centered differencing is applied to calculate $\partial\theta/\partial p$.

APPENDIX B

Procedures Used in Determining the Basic Field

Given the basic azimuthal flow V and its radial variation [Eq. (2.9)] at the 900 mb level, the basic radial flow U and the vertical p-velocity W are determined by the following procedures. In this Appendix, the suffix 9 and 10 will be used to denote the quantities at the 900 and 1000 mb levels, respectively. The 900 mb level is assumed to be the top of the planetary boundary layer.

The numerical results from the tropical cyclone simulation model (Kurihara, 1975) suggest that, at mature stage of a tropical cyclone, the torque due to the difference in the radial forces $fV+V^2/R$ at the 900 and 1000 mb levels is approximately counteracted by the torque caused by the difference in the frictional forces at the corresponding two levels. This balance condition gives the relationship among V_9, V_{10} and F_{10}, where F is the frictional force and F_9 is assumed to be negligible. Accordingly, if the relation between V_9 and V_{10} and between F_{10} and U_{10} are found, then V_{10} and U_{10} can be derived from V_9. Figs. B1 and B2 illustrate each of these relations for data from the numerical simulation experiment (Kurihara, 1975). In the present study, the empirical relations drawn from these two figures are used, namely,

$$|V_{10}| = 1.16|V_9|^{0.824}, \tag{B1}$$

where V is in m s^{-1} and V_{10} has the same sign with V_9, and

$$|U_{10}| = 186.6|F_{10}|^{0.463}, \tag{B2}$$

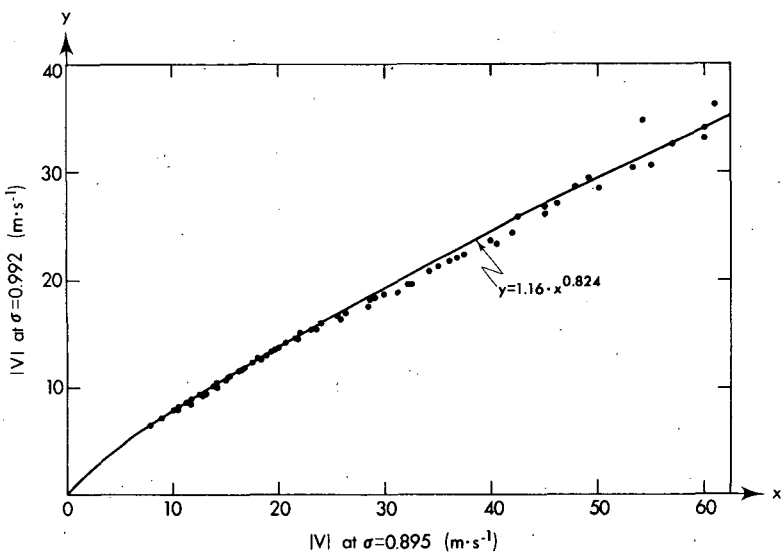

FIG. B1. Scatter diagram of $|V|$ at $\sigma=0.992$ and $\sigma=0.895$ (σ=pressure normalized by the surface value). Data are taken from the numerical results for the radius range 60 through 700 km in a simulated mature tropical cyclone (Kurihara, 1975). The curve indicates the empirical relation used in the present study.

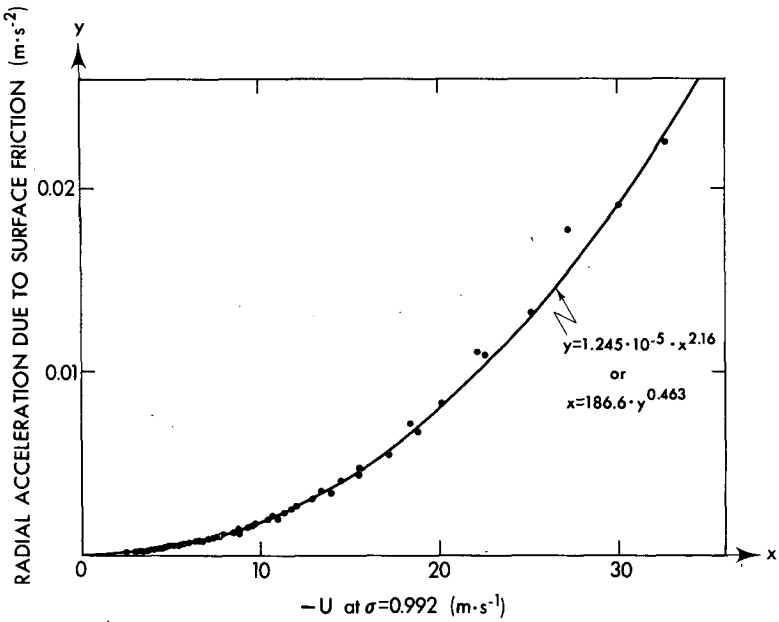

FIG. B2. Scatter diagram of the frictional force at the surface and $-U$ at $\sigma=0.992$. See Fig. B1 for further explanation.

where U is in m s^{-1}, F is in m s^{-2} and the sign of U_{10} is opposite to that of F_{10}.

The vertical profile of U is specified by assuming an exponential variation with pressure in the boundary layer and in an upper layer ($p \leqslant 100$ mb) and a linear variation with p between these layers:

$$U(p)=U_{10}I(p), \tag{B3}$$

where

$$I(p)=\begin{cases}\exp\left(-\dfrac{1000-p}{40}\right) & \text{for } 900\leqslant p\leqslant 1000\\ \left(-1+\dfrac{p-100}{400}\right)\exp\left(-\dfrac{100}{40}\right) & \text{for } 100<p<900\\ -\exp\left(-\dfrac{p}{40}\right) & \text{for } 0<p\leqslant 100.\end{cases}$$

In (B3), the factor 40 is chosen so that the thickness of the boundary layer becomes approximately 100 mb. $I(p)$ is asymmetric with respect to the 500 mb level, where it is zero.

Eq. (2.9) in the main text yields $(\partial V/\partial r)_9$. Then $(\partial V/\partial r)_{10}$ can be derived from (B1). The result is equivalent to taking $\lambda_{10}=0.824\lambda_9$ in (2.9). It is not difficult to calculate $(\partial U/\partial r)_{10}$, for the given $(\partial V/\partial r)_9$ and $(\partial V/\partial r)_{10}$, with the application of the balance condition for the torque in the boundary layer as mentioned before and also with the use of (B2). In this study, $\partial U/\partial r$ at other levels are determined by the relation $\partial U/\partial r=(\partial U/\partial r)_{10}I(p)$ where $I(p)$ is the same function as defined by (B3).

Finally, the vertical p-velocity is calculated by integrating the continuity equation with the boundary condition $W=0$ at $p=0$ mb:

$$W(p)=-\left(\frac{\partial U}{\partial r}+\frac{U}{R}\right)_{10}\int_0^p I(p)dp. \tag{B4}$$

Since $I(p)$ is asymmetric with respect to the 500 mb level, it follows that W vanishes at $p=1000$ mb.

REFERENCES

Abdullah, A. J., 1966: The spiral bands of a hurricane: A possible dynamic explanation. *J. Atmos. Sci.*, **23**, 367–375.

Anthes, R. A., 1972: Development of asymmetries in a three-dimensional numerical model of the tropical cyclone. *Mon. Wea. Rev.*, **100**, 461–476.

Arakawa, H., and D. Manabe, 1963: Investigation of spiral rain bands and frontal structures in terms of shallow water waves. *Pap. Meteor. Geophys.*, **14**, 127–143.

Atlas, D., K. R. Hardy, R. Wexler and R. J. Boucher, 1963: On the origin of hurricane spiral bands. *Geofis. Intern.*, **3**, 123–132.

Diercks, J. W., and R. A. Anthes, 1975: Generation, propagation, and maintenance of spiral bands in linear and nonlinear hurricane models. Presented at the Ninth Technical Conference on Hurricanes and Tropical Meteorology, Key Biscayne, Fla., Amer. Meteor. Soc.

Faller, A. J., 1961: An experimental analogy to and proposed explanation of hurricane spiral bands. *Preprints Second Tech. Conf. Hurricanes*, Amer. Meteor. Soc., 307–313.

Fett, R. W., 1964: Aspects of hurricane structure. New model consideration suggested by TIROS and Project Mercury observations. *Mon. Wea. Rev.*, **92**, 43–60.

Fujita, T., T. Izawa, K. Watanabe and I. Imai, 1967: A model of typhoons accompanied by inner and outer rainbands. *J. Appl. Meteor.*, **6**, 3–19.

Jordan, C. L., 1958: Mean soundings for the West Indies area. *J. Meteor.*, **15**, 91–97.

Kurihara, Y., 1975: Budget analysis of a tropical cyclone simulated in an axisymmetric numerical model. *J. Atmos. Sci.*, **32**, 25–59.

——, and R. E. Tuleya, 1974: Structure of a tropical cyclone developed in a three-dimensional numerical simulation model. *J. Atmos. Sci.*, **31**, 893–919.

Lamb, H., 1932: *Hydrodynamics*. Dover, 738 pp.

Ligda, M. G. H., 1955: Hurricane squall lines. *Bull. Amer. Meteor. Soc.*, **36**, 340–342.

Mathur, M. B., 1975: Development of banded structure in a numerically simulated hurricane. *J. Atmos. Sci.*, **32**, 512–522.

Riehl, H., and J. S. Malkus, 1961: Some aspects of hurricane Daisy, 1958. *Tellus*, **13**, 181–213.

Senn, H. V., and H. W. Hiser, 1959: On the origin of hurricane spiral rain bands. *J. Meteor.*, **16**, 419–426.

Simpson, R. H., 1954: Structure of an immature hurricane. *Bull. Amer. Meteor. Soc.*, **35**, 335–350.

Staff Members, Tokyo University, 1969: Precipitation bands of Typhoon Vera in 1959 (Part I). *J. Meteor. Soc. Japan*, **47**, 298–309.

——, 1970: Precipitation bands of Typhoon Vera in 1959 (Part II). *J. Meteor. Soc. Japan*, **48**, 103–117.

Tatehira, R., 1961: A mesosynoptic and radar analysis of typhoon rain band, case study of typhoon "Helen," 1958. *Proc. Second Tech. Conf. Hurricanes*, Amer. Meteor. Soc., 115–126.

Tepper, M., 1958: A theoretical model for hurricane radar bands. *Preprints Seventh Weather Radar Conf.*, Miami, Amer. Meteor. Soc., K56–65.

Tuleya, R. E., and Y. Kurihara, 1975: The energy and angular momentum budgets of the three-dimensional tropical cyclone model. *J. Atmos. Sci.*, **32**, 287–301.

Wexler, H., 1947: Structure of hurricanes as determined by radar. *Ann. N. Y. Acad. Sci.*, **48**, 821–844.

Yamasaki, M., 1969: Large-scale disturbances in the conditionally unstable atmosphere in low-latitudes. *Pap. Meteor. Geophys.*, **20**, 289–336.